SIMULATION MODEL FOR THE PIPER PA-30 LIGHT MANEUVERABLE AIRCRAFT IN THE FINAL APPROACH

JOSEPH S. KOZIOL JR.
TRANSPORTATION SYSTEM CENTER
55 BROADWAY
CAMBRIDGE, MA.02142

JULY 1971
TECHNICAL MEMORANDUM

Prepared for

FAA/SRDS
800 INDEPENDENCE AVENUE S.W.
WASHINGTON,D.C. 20590

1. Report No. DOT-TSC-FAA-71-11	2. Government Accession No.	3. Recipient's Catalog No.	
4. Title and Subtitle SIMULATION MODEL FOR THE PIPER PA-30 LIGHT MANEUVERABLE AIRCRAFT IN THE FINAL APPROACH		5. Report Date June, 1971	
		6. Performing Organization Code	
7. Author(s) Joseph S. Koziol, Jr.		8. Performing Organization Report No.	
9. Performing Organization Name and Address TRANSPORTATION SYSTEMS CENTER 55 BROADWAY CAMBRIDGE, MASS. 02142		10. Work Unit No.	
		11. Contract or Grant No.	
12. Sponsoring Agency Name and Address FAA/SRDS 800 Independence Avenue, S. W. Washington, D. C. 20590		13. Type of Report and Period Covered TECHNICAL MEMORANDUM	
		14. Sponsoring Agency Code	
15. Supplementary Notes			

16. Abstract

This report describes the Piper PA-30 "Twin Comanche" aircraft and a representative autopilot during the final approach configuration for simulation purposes. The aircraft is modeled by linearized six—degree—of—freedom perturbation equations referenced to the aircraft stability axis. Other equations are presented which derive the body axis rates, velocities and accelerations, and ground referenced velocities (translation equations).

The autopilot is a representative system for automatic ILS approaches from initial localizer track down to decision height. The glideslope system is engaged by approaching the glidepath at constant altitude (usually in the altitude hold mode) on the localizer beam. The pilot must take over manually at the decision height since light aircraft are not normally equipped with automatic flare capability.

The aircraft autopilot model described herein has been used extensively in simulation studies at TSC and exhibits the expected behavior.

17. Key Words Light maneuverable aircraft, autopilot model, final approach, simulation studies	18. Distribution Statement Unclassified – Unlimited		
19. Security Classif. (of this report) Unclassified	20. Security Classif. (of this page) Unclassified	21. No. of Pages 21	22. Price

TABLE OF CONTENTS

LIST OF ILLUSTRATIONS

SYMBOLS

a_n	measured normal acceleration at accelerometer station	ft/sec^2
b	wing span	ft.
BHP	engine brake horsepower	-
c	mean aerodynamic chord	ft.
C_D	drag coefficient	-
$C_{D()}$	nondimensional drag stability derivative	-
$C_{ha()}$	nondimensional aileron hinge-moment coefficient	-
$C_{he()}$	nondimensional elevator hinge-moment coefficient	-
$C_{hr()}$	nondimensional rudder hinge-moment coefficient	-
C_L	lift coefficient	-
$C_{L()}$	nondimensional lift stability derivative	-
C_ℓ	rolling-moment coefficient	-
$C_{\ell()}$	nondimensional rolling-moment stability derivative	-
C_m	pitching-moment coefficient	-
$C_{m()}$	nondimensional pitching-moment stability derivative	-
C_n	yawing-moment coefficient	-
$C_{n()}$	nondimensional yawing-moment stability derivative	-
C_Y	side-force coefficient	-
$C_{Y()}$	nondimensional side-force stability derivative	-

C_T	thrust coefficient	-
g	gravity constant	ft/sec^2
h	aircraft altitude referenced to sea level	ft.
$I_{xx()}$	aircraft rolling moment of inertia	slug-ft^2
$I_{yy()}$	aircraft pitching moment of inertia	slug-ft^2
$I_{zz()}$	aircraft yawing moment of inertia	slug-ft^2
$I_{xz()}$	aircraft product of inertia	slug-ft^2
m	mass of aircraft	slugs
MAP	engine absolute manifold pressure	in. of Hg
N_P	engine power efficiency	-
$P_{()}$	rolling angular rate of aircraft (about stability axis when no subscript)	rad/sec
$q_{()}$	pitching angular rate of aircraft (about stability axis when no subscript)	rad/sec
$\bar{q}$	free-stream dynamic pressure	lbs/ft^2
r	yawing angular rate of aircraft (about stability axis when no subscript)	rad/sec
r.p.m.	engine revolutions per minute	-
S	wing area	ft^2
T	effective thrust	lbs.
ΔT	change in thrust due to pilot throttle input	lbs.
$u_{()}$	perturbed forward velocity of aircraft (along stability x-axis when no subscript)	ft/sec
U_o	equilibrium or reference forward velocity of aircraft	ft/sec
$v_{()}$	perturbed side velocity of aircraft (along atability Y-axis when no subscript)	ft/sec
V_T	total velocity of aircraft	knots

$w_{()}$	perturbed normal velocity of aircraft (along stability Z axis when no subscript)	ft/sec
x_{accel}	distance from center of gravity to accelerometer location measured along X fuselage axis, positive forward	ft.
X_E	X-axis in local vertical coordinate frame	–
Y_E	Y-axis in local vertical coordinate frame	–
Z_E	Z-axis in local vertical coordinate frame	–
Z_T	pitching moment arm of the thrust vector positive downward	ft.
α	angle of attack = $\tan^{-}(w/u)$	rad.
α_r	angle between X-stability axis and fuselage axis	rad.
α_T	angle between X-stability axis and thrust axis	rad.
β	angle of sideslip = $\sin^{-}(v/V_T)$	rad.
ε	glideslope error, localizer error	rad.
δ_t	deflection of throttle position ($\delta_t = 1$ = full throttle)	–
$\delta_{()}$	deflection of control surface	rad.
θ, ϕ, ψ	Euler angles referenced to stability axis	rad.
ρ	atmospheric air density	slug/ft^3
$(\cdot)$	derivative with respect to time	–

Subscripts

a	aileron
B	fuselage reference frame
E	local vertical coordinate frame
e	elevator or stabilizer
f	flaps

ix

o   equilibrium or reference condition

r   rudder

s   aircraft stability coordinate frame

t   throttle

$u, \alpha, q, \theta, r, p$ $\delta_e, \delta_a, \delta_r$ as defined above

1.0 INTRODUCTION

The primary objective of this research effort is to derive a light, maneuverable aircraft-autopilot model as one extreme of aircraft type for final approach simulation studies. This model is to serve as a high priority vehicle in two FAA projects: developing requirements for a Scanning Beam Microwave Instrument Landing System and developing an all-encompassing generalized set of equations of an aircraft during approach and landing for all-weather landing system studies on the NAFEC hybrid computation facility.

In general, no such model existed for a common and representative light aircraft at the beginning of this effort because light aircraft are not generally designed by analysis and simulation. Similarly, light aircraft generally do not have automatic landing systems as standard equipment.

The definition and identification of a light maneuverable aircraft is treated in Reference (1). The Piper PA-30 "Twin Comanche" is selected as the light maneuverable aircraft for modeling primarily because of the availability of data from wind tunnel and actual flight tests and because of an existing, partially useful, simulation model at the NASA Edwards Flight Research Center. The final aircraft model is derived from this simulation model and NASA TN D4983. The flight condition is based upon a high wind environment (headwind and sidewind of approximately 24 feet per second). This condition was selected to represent an extreme case for the simulation studies.

The autopilot description is based on a report (Reference 6) prepared for TSC by Dr. Kohlman of the University of Kansas. The final configuration (i.e., gain values, gain scheduling and logic) was determined by simulation at TSC.

2.0 VEHICLE DESCRIPTION [4]

The Piper PA-30 is a light twin engine low-wing monoplane.
Figure 1 gives the principal dimensions. The airplane has a
wing span of 35.98 ft., a wing area of 178 ft^2, an aspect ratio
of 7.3, and a mean aerodynamic cord of 5 feet based on projec-
tion of the outboard leading edge of the wing through the fuse-
lage. The wing airfoil section is a modified NACA64_2A215 air-
foil with the trailing-edge cusp faired out. The wing has 5° of
dihedral with no twist and is at 2° positive incidence with
respect to the fuselage reference line. The airplane has the
standard three-control system. The horizontal tail is of the
all-movable type with a control deflection range of 4° to -14°.
The tail has a trailing-edge tab which moves in the same direc-
tion as the tail with a deflection ratio (tab deflection to tail
deflection) of 1.5. The control deflection range on each aileron
is from 14° to -18°. The rudder control deflection range is
±27°.

2.1 Vehicle Model

A final approach model is presented for the Piper PA-30
aircraft based on data available from the NASA Edwards Flight
Research Center simulation model and NASA TND 4983. The model
consists of rigid body, six-degree-of-freedom aircraft equations
of motion which are basically linear perturbation equations in
the stability axis system (some of the nonlinear cross coupling
terms have been included).

2.2 Axis Systems

The stability axis frame (s) is depicted in Figure 2. The
definition of airplane angles and sign convention is described
in Figure 3. The stability axis is fixed to the aircraft and
rotates and translates with the aircraft. Its origin is the
center of mass of the aircraft. The X-axis is in the direction
of motion of the airplane in a reference condition of steady

-2-
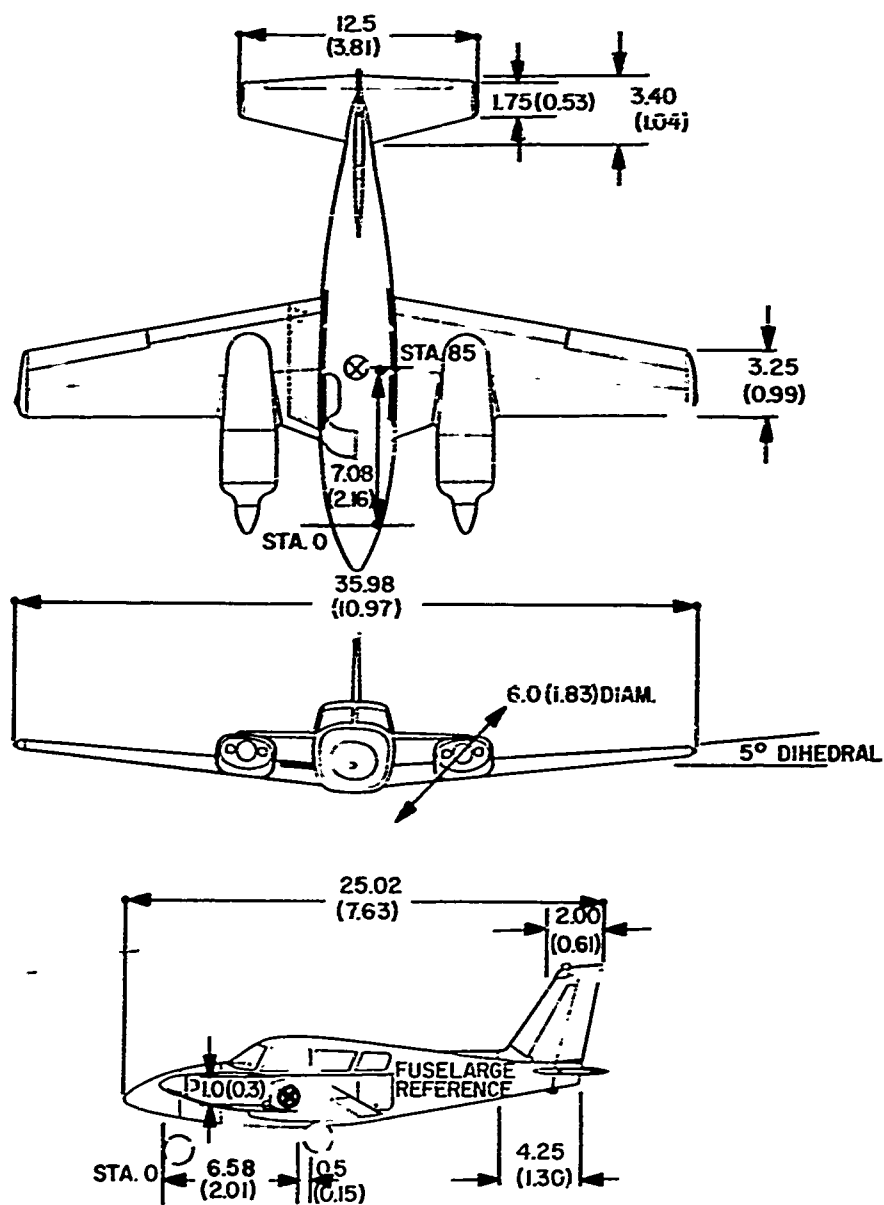
All dimensions are in feet (meters).

Figure 1.   Piper Dimensional Data[4]
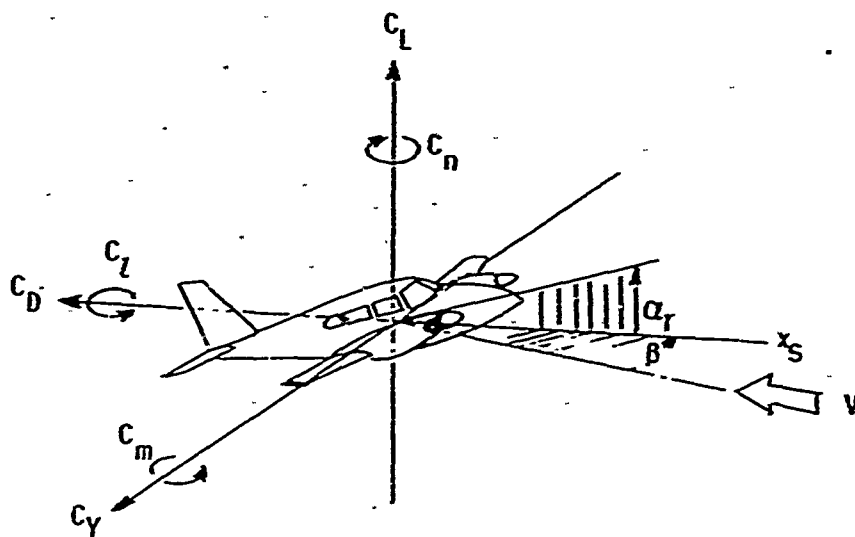
Figure 2. System of Axes and Positive
           Sense of Angles, Forces and Moments[4]

-4-
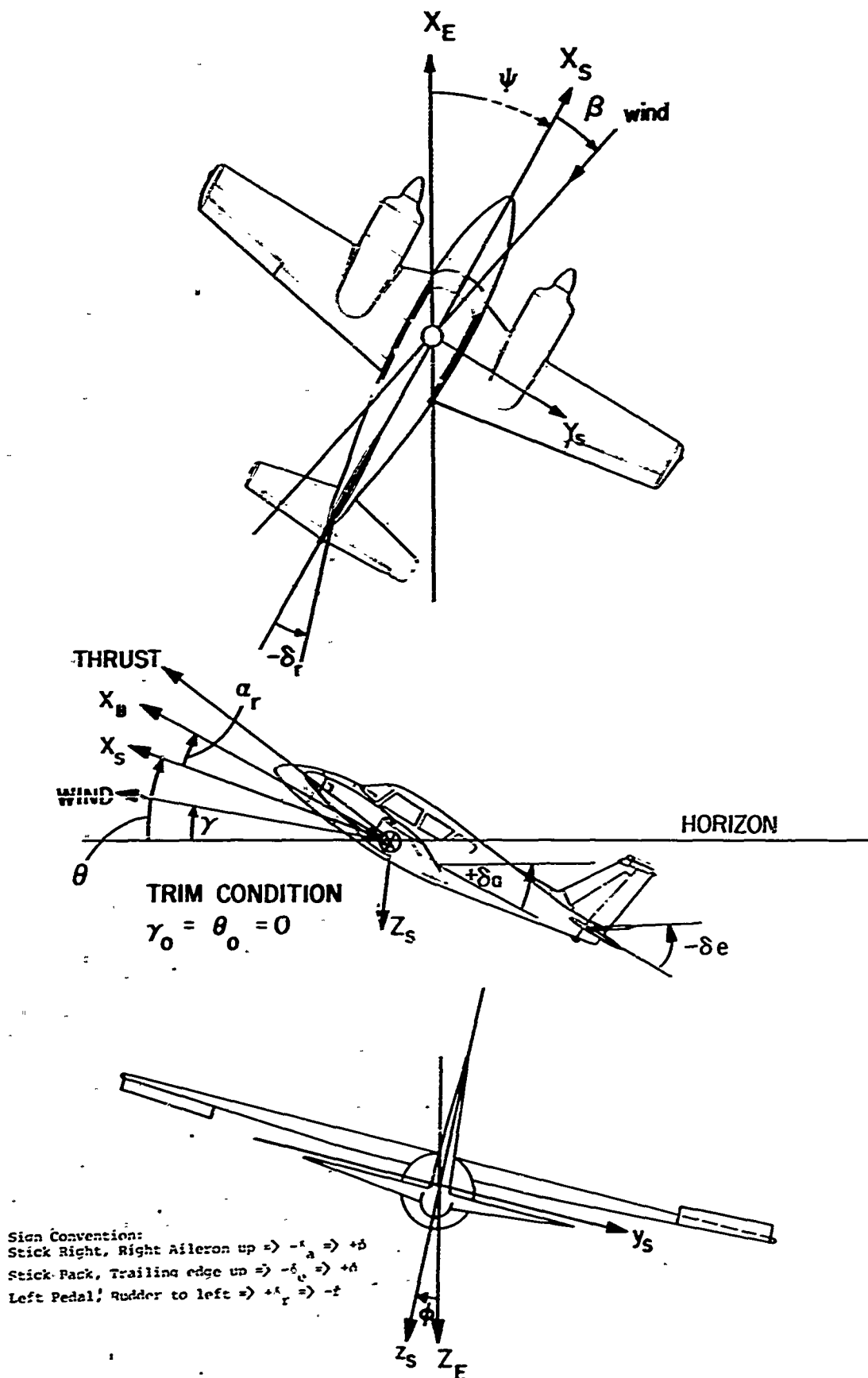
Figure 3. Definition of Airplane
Angles and Sign Convention

Sign Convention:
Stick Right, Right Aileron up => $-\delta_a$ => $+\delta$
Stick Back, Trailing edge up => $-\delta_e$ => $+\theta$
Left Pedal, Rudder to left => $+\delta_r$ => $-\psi$

symmetric flight. The Y-axis is normal to the aircraft's plane of symmetry (positive to the right), and the Z-axis is in the plane of symmetry (positive downward) and orthogonal to the X- and Z-axes. The aerodynamic stability derivatives are all referenced to this axis system.

A fuselage referenced body coordinate frame (B), is defined for determining the angular rates and velocities in body axis, and the aircraft normal acceleration. This axis system is similar to the stability axis system except that the X-axis is directed along the fuselage. The angle α_r relates the two axis systems. A local vertical coordinate frame (E) is defined for determining the velocities of the aircraft with respect to the air mass. This coordinate frame has its origin at the center of mass of the aircraft with the X-axis pointing North, and Y-axis pointing East, and the Z-axis pointing down. The velocities from this coordinate frame can be converted to ground velocity by adding the various components of the steady wind.

2.3 Assumptions in Using Aircraft Equations

The derivation of the aircraft equations involved the following assumptions:

1. Aircraft mass is constant.
2. The earth can be considered an inertial frame.
~   The aircraft is a rigid body.
4. The aircraft is symmetrical about its X-Z plane.
5. The aircraft is initially in equilibrium flight with no linear or angular accelerations, no angular rates, and no initial roll angle or lateral velocity.
6. Small disturbance (perturbation) theory is used. Motions and forces are referred to the equilibrium flight condition.
7. Hinge moments are insignificant.

2.4 Equations of Motion

Drag Equation

$$\frac{m}{\bar{q}S}\,\dot{u} + \frac{2C_{D_o}}{U_o}\,u - \left(C_{L_o}-C_{D_\alpha}\right)\alpha + \frac{mg}{\bar{q}S}\,\theta - \frac{mU_o}{\bar{q}S}\,r\beta = \frac{\left(\cos\alpha_T\right)}{\bar{q}S}\Delta T$$

Lift Equation

$$\frac{2C_{L_o}}{U_o}\,u + \left(\frac{mU_o}{\bar{q}S} + \frac{c}{2U_o}C_{L_{\dot\alpha}}\right)\dot\alpha + \left(C_{L_\alpha} + C_{D_o}\right)\alpha + \left(\frac{c}{2U_o}C_{L_q} - \frac{mU_o}{\bar{q}S}\right)q$$

$$+ \left(\frac{mg}{\bar{q}S}\,\theta_o\right)\theta + \frac{mU_o}{\bar{q}S}\,\beta\rho - \frac{m}{\bar{q}S}\,qu = -\,C_{L_{\delta_e}}\delta_e - \frac{\left(\sin\alpha_T\right)}{\bar{c}S}\Delta T$$

Pitching Moment Equation

$$-\frac{C_{m_u}}{U_o}\,u - \frac{c}{2U_o}C_{m_{\dot\alpha}}\dot\alpha - C_{m_\alpha}\alpha + \frac{I_{YY_S}}{\bar{q}Sc}\,\dot{q} - \frac{c}{2U_o}C_{m_q}q = C_{m_{\delta_e}}\delta_e + \frac{z_T}{\bar{q}Sc}\Delta T$$

Sideforce Equation

$$\frac{mU_o}{\bar{q}S}\,\dot\beta - C_{Y_\beta}\beta - \frac{b}{2U_o}C_{Y_p}p - \frac{mg}{\bar{q}S}\,\phi + \frac{mU_o}{\bar{q}S}\,r - \frac{b}{2U_o}C_{Y_r}r + \frac{m}{\bar{q}S}\,ru =$$

$$C_{Y_{\delta r}}\delta r + C_{Y_{\delta a}}\delta a$$

Rolling Moment Equation

$$-\,C_{\ell_\beta}\beta + \frac{I_{xx_S}}{\bar{q}Sb}\,\dot{p} - \frac{b}{2U_o}C_{\ell_p}p - \frac{I_{xz_S}}{\bar{q}Sb}\,\dot{r} - \frac{b}{2U_o}C_{\ell_r}r = C_{\ell_{\delta r}}\delta r + C_{\ell_{\delta a}}\delta a$$

Yawing Moment Equation

$$-\,C_{n_\beta}\beta - \frac{I_{xz_S}}{\bar{q}Sb}\,\dot{p} - \frac{b}{2U_o}C_{n_p}p + \frac{I_{zz_S}}{\bar{q}Sb}\,\dot{r} - \frac{b}{2U_o}C_{n_r}r = C_{n_{\delta r}}\delta r + C_{n_{\delta a}}\delta a$$

Body Axis Rates and Velocities

$$q_B = q$$

$$p_B = p \cos(\alpha_r) - r \sin(\alpha_r)$$

$$r_B = r \cos(\alpha_r) + p \sin(\alpha_r)$$

$$u_B = (U_O + u) \cos(\alpha_r) - U_O \alpha \sin(\alpha_r)$$

$$w_B = U_c \alpha \cos(\alpha_r) + (U_O + u) \sin(\alpha_r)$$

$$v_B = U_O \beta$$

Accelerations

Vertical acceleration at center of gravity

$$\dot{w}_B = U_O \dot{\alpha} \cos(\alpha_r) + \dot{u} \sin(\alpha_r)$$

Vertical acceleration at accelerometer

$$\dot{w}_{accel} = \dot{w}_B - x_{accel} \, \dot{q}$$

Measured Normal Acceleration

$$a_n = \dot{w}_{accel} + p_B v_B - q_B U_B$$

Euler Angle Rates

$$\dot{\theta} = q \cos \Phi - r \sin \Phi$$

$$\dot{\Phi} = p + (q \sin \Phi + r \cos \Phi) \tan \theta$$

$$\dot{\psi} = (q \sin \Phi + r \cos \Phi) \sec \theta$$

8

Translation Equations With Respect to Moving Frame

$$\dot{X}_E = (U_0+u)\cos\theta\cos\psi + U_0\beta(\sin\phi\sin\theta\cos\psi - \cos\phi$$
$$\sin\psi) + U_0\alpha(\cos\phi\sin\theta\cos\psi + \sin\phi\sin\psi)$$

$$\dot{Y}_E = (U_0+u)\cos\theta\sin\psi + U_0\beta(\sin\phi\sin\theta\sin\psi + \cos\phi$$
$$\cos\psi) + U_0\alpha(\cos\phi\sin\theta\sin\psi - \sin\phi\cos\psi)$$

$$\dot{Z}_E = (U_0+u)(-\sin\theta) + U_0\beta\sin\phi\cos\theta + U_0\alpha\cos\phi\cos\theta.$$

2.5 Vehicle Data

Geometry

b = 35.98 ft.

c = 5. ft.

S = 178. ft.^{2}

Z_T = -.75 ft.

α_T = 0 deg.

Weight and Inertias

$m = 111.9$ slugs $\quad I_{xxB} = 2800$ slug-ft^2 $\quad I_{xxs} = 2801.7$ slug-ft^2

$I_{yyB} = 1900$ slug-ft^2 $\quad I_{yys} = 1900.$ slug-ft^2

$I_{zzB} = 4500$ slug-ft^2 $\quad I_{zzs} = 4513.7$ slug-ft^2

$I_{xzB} = 80$ slug-ft^2 $\quad I_{xzs} = -7.9$ slug-ft^2

Trim Flight Condition - Final Approach (High Wind Environment)

$U_0 = 176.$ ft/sec $\qquad\qquad$ o = .002378 slugs/ft^3

$C_{LO} = .55$ $\qquad\qquad\qquad$ $\bar{q}$ = 36.8 lbs/ft^2

$C_{DO} = .034$ $\qquad\qquad\qquad$ α_r = .0515 rad (2.95°)

$\theta_0 = 0.^\circ$

$\gamma_0 = 0.^\circ$ $\qquad\qquad\qquad$ C_T (thrust coeff.) $\cong$ .034

δ_e (trim elevator setting) = 0.4° $\qquad$ center of gravity at 10% MAC

δ_f (trim flap setting)   = 0.$^\circ$ $\qquad$ gear down

9

Non-Dimensional Derivatives - Final Approach

$C_{D_u} = 0.$ $C_{L_u} = 0.$ $C_{m_u} = 0.$

$C_{D_\alpha} = .275$ $C_{L_\alpha} = 5.04$ $C_{m_\alpha} = -1.147$

$C_{D_{\dot\alpha}} = 0.$ $C_{L_{\dot\alpha}} = 5.3$ $C_{m_{\dot\alpha}} = -14.55$

$C_{D_q} = 0.$ $C_{L_q} = 9.12$ $C_{m_q} = -25.0$

$C_{D_{\delta e}} = 0.$ $C_{L_{\delta e}} = 1.05$ $C_{m_{\delta e}} = -2.87$

$C_{\ell_\beta} = -.086$ $C_{n_\beta} = .0756$ $C_{Y_\beta} = -.494$

$C_{\ell_r} = .11$ $C_{n_r} = -.16$ $C_{Y_r} = 0.$

$C_{\ell_p} = -.50$ $C_{n_p} = -.063$ $C_{Y_p} = 0.$

$C_{\ell_{\delta r}} = .01147$ $C_{n_{\delta r}} = -.0573$ $C_{Y_{\delta r}} = .143$

$C_{\ell_{\delta a}} = -.0803$ $C_{n_{\delta a}} = .00573$ $C_{Y_{\delta a}} = -.00916$

2.6 Control Wheel and Pedal Characteristics

Aileron: Gearing constant at zero control deflection,
             0.80 radian/ft.; wheel deflection, $\pm 90^\circ$; max.
             force at end of wheel, ± 15 lb.

Elevator: Gearing constant at zero control deflection,
             0.42 radian/ft.; wheel throw, 4 inches forward,
             5 inches aft; force differential 40 lbs.
             (detent position is 4 inches from firewall)

Rudder: Gearing constant at zero control deflection,
             0.93 radian/ft.; pedal deflection, 4 1/2 inches;
             maximum force at full deflection, 120 lbs.

3. ENGINE THRUST DATA

Two 160 h.p. Lycoming IO-320-B four-cylinder air-cooled engines power the PA-30. Figure 4 presents the maximum available manifold pressure from each engine as a function of standard temperature altitude. This curve should be mechanized so that the pilot's indicator shows the maximum value as a function of altitude at full throttle.

Figure 5 presents the power available per engine as a function of r.p.m., MAP, and altitude. This curve should be mechanized so that power can be obtained from the r.p.m., MAP, and altitude.

Once the power is obtained, thrust can be calculated from the following equation:

$$T \text{ (lbs.)} = \frac{325 \ N_p \ BHP}{V_T \text{(knots)}}$$

where N_p (power efficiency) = 0.74

Alternatively, a simplified algebraic expression for BHP has been derived from Figure 5 for the final approach configuration and can be used in place of Figure 5. The expression is given by

$$BHP = .0024(h) + .0028(r.p.m.) \left\{ \left[\delta_t \left(29.2 - .000989(h) \right) \right] - 8.0 \right\}$$

where h = altitude in feet

$\delta_t = 1$ = full throttle

An engine lag of about 0.1 second can be used in completing the engine transfer function (i.e. throttle→thrust).
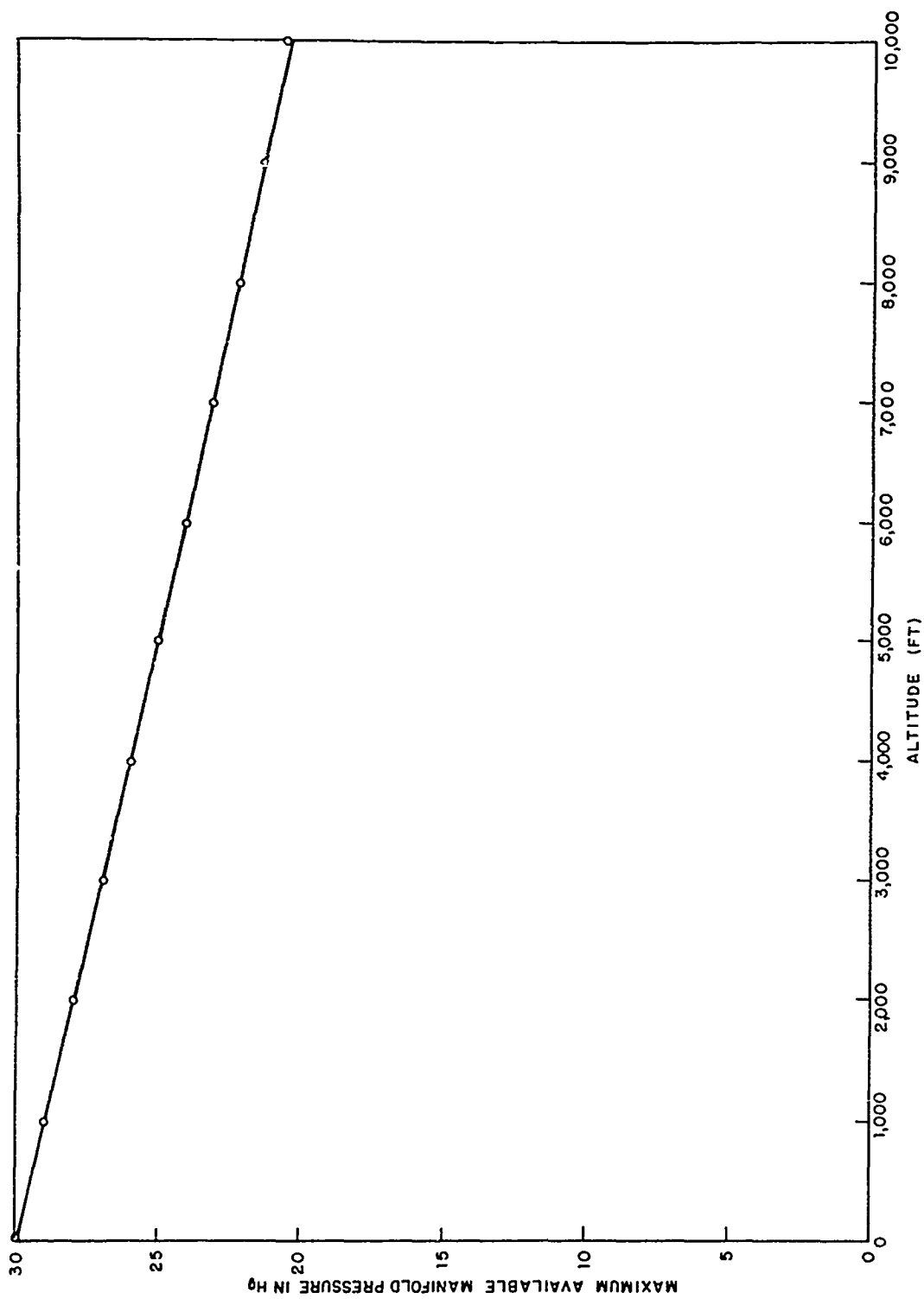
Figure 4. Maximum Available Manifold Pressure

TO FIND ACTUAL HORSEPOWER FROM ALTITUDE, r.p.m., AND MANIFOLD PRESSURE:

1. LOCATE A ON FULL THROTTLE ALTITUDE CURVE FOR GIVEN r.p.m. MANIFOLD PRESSURE.
2. LOCATE B ON SEA LEVEL CURVE FOR r.p.m. & MANIFOLD PRESSURE & TRANSFER TO C.
3. CONNECT A & C BY STRAIGHT LINE AND READ HORSEPOWER AT GIVEN ALTITUDE D.

PRESSURE ALTITUDE IN THOUSANDS OF FEET

BRAKE HORSEPOWER AT STD TEMP AND PRESS
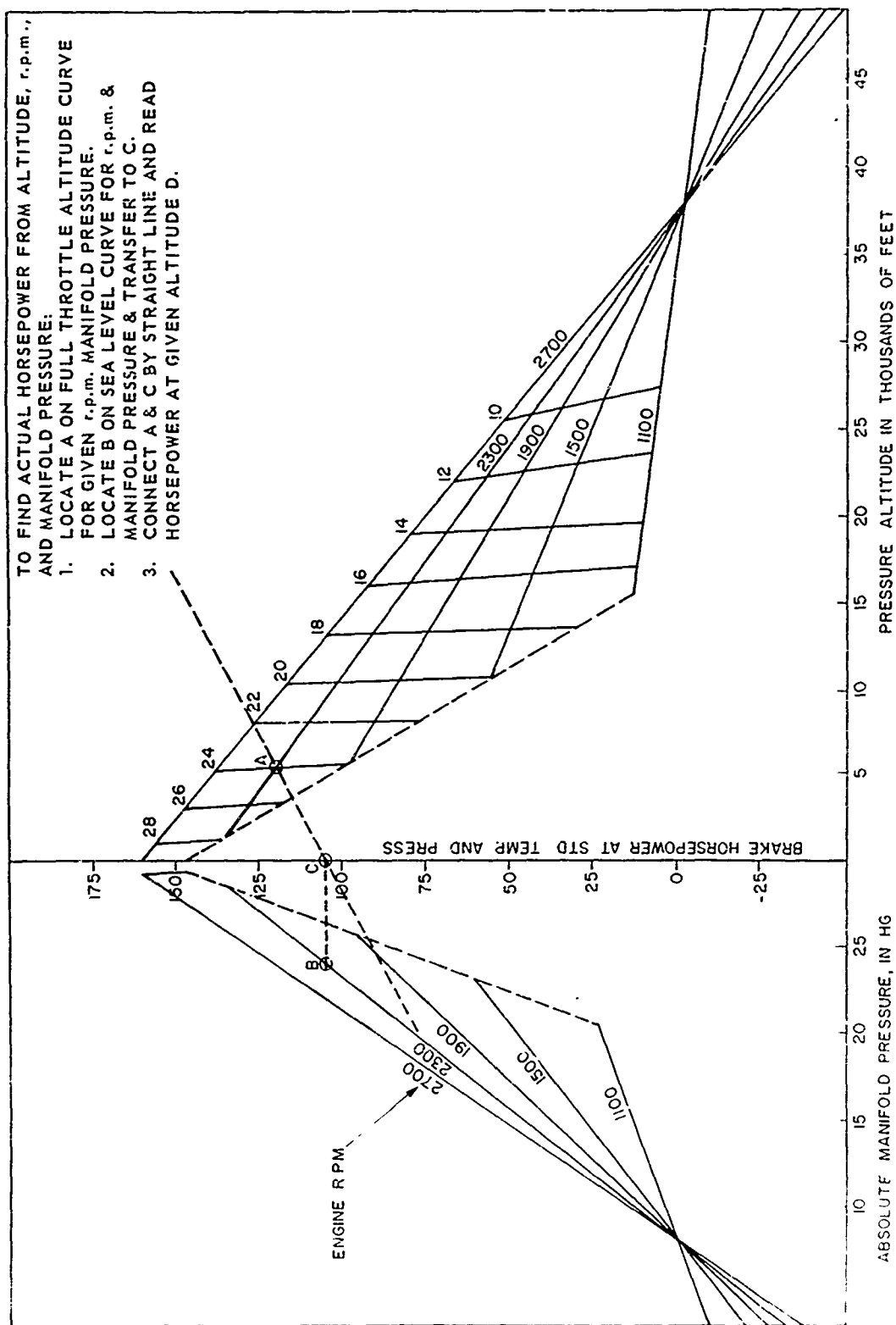
ABSOLUTE MANIFOLD PRESSURE, IN HG

ENGINE R PM

Figure 5.   Power Characteristics Per Engine

4. AUTOPILOT

This section describes a representative PA-30 three-axis
autopilot with stabilization system and with an automatic ILS ap-
proach mode available down to decision height.

Block diagrams of the longitudinal and lateral axis are shown
in Figures 6 and 7 respectively. Damping is provided about all
three axes, and inputs to the system come from a vertical gyro
(θ, ϕ), yaw rate gyro (r), altitude sensor, and navigation receiver.
Limiters are installed in the lateral channel to prevent exces-
sive roll angles in response to large error signals. Gain schedul-
ing is provided in the longitudinal channel to desensitize the
system to glidepath errors as the runway threshold is approached.
Automatic ILS approaches are possible down to decision height.
The pilot must take over manually at that point because there is
no automatic flare capability.

The auto-trim system, which actuates the elevator trim tab to
unload the elevator servo, is not included in the block diagrams
since it has no measurable influence on the performance or dynamic
response of the airplane-autopilot system. It is a time-delayed,
slow, integrating actuator and as such does not respond to tran-
sients.

The output of the autopilot system is expressed in control
surface deflections. Because of the dependence of deflections on
dynamic pressure, the final gain of $1/\bar{q}$ represents the aerodynamic
gain of the control surfaces.

The glideslope system is engaged by approaching the glidepath
at constant altitude (usually in the altitude hold mode) on the
localizer beam. Initially the glideslope error signal will be a
strong nose up command but switch B will be open. The "glideslope
engage logic" circuit continuously monitors the signal at point B,
which will gradually decrease in strength as the glidepath is ap-
proached. When the signal at point B reaches a 0.044 rad. (2.5°)
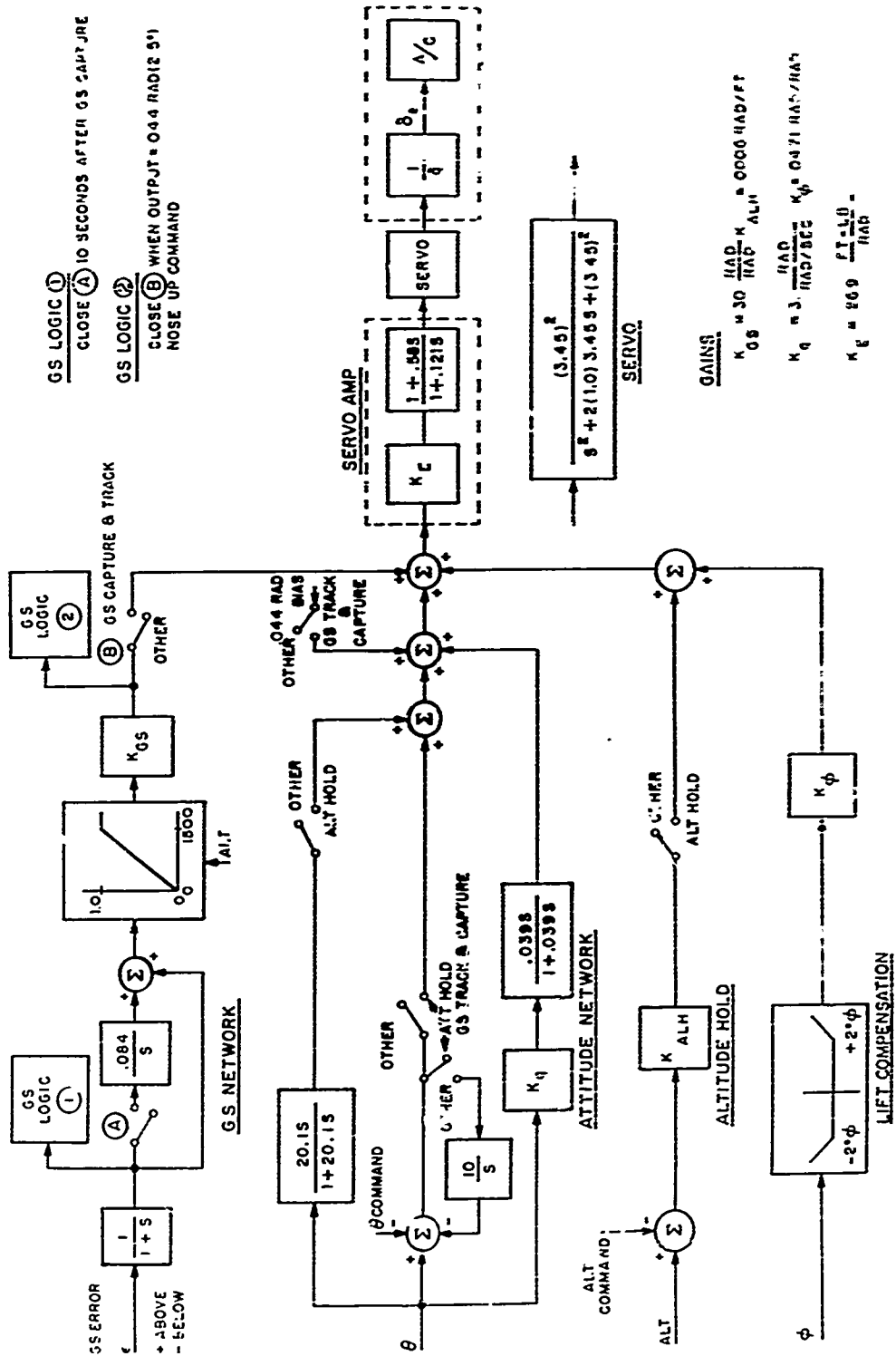nose up command, switch B is closed, and the altitude hold mode is

-14-

Figure 6. Longitudinal Control System
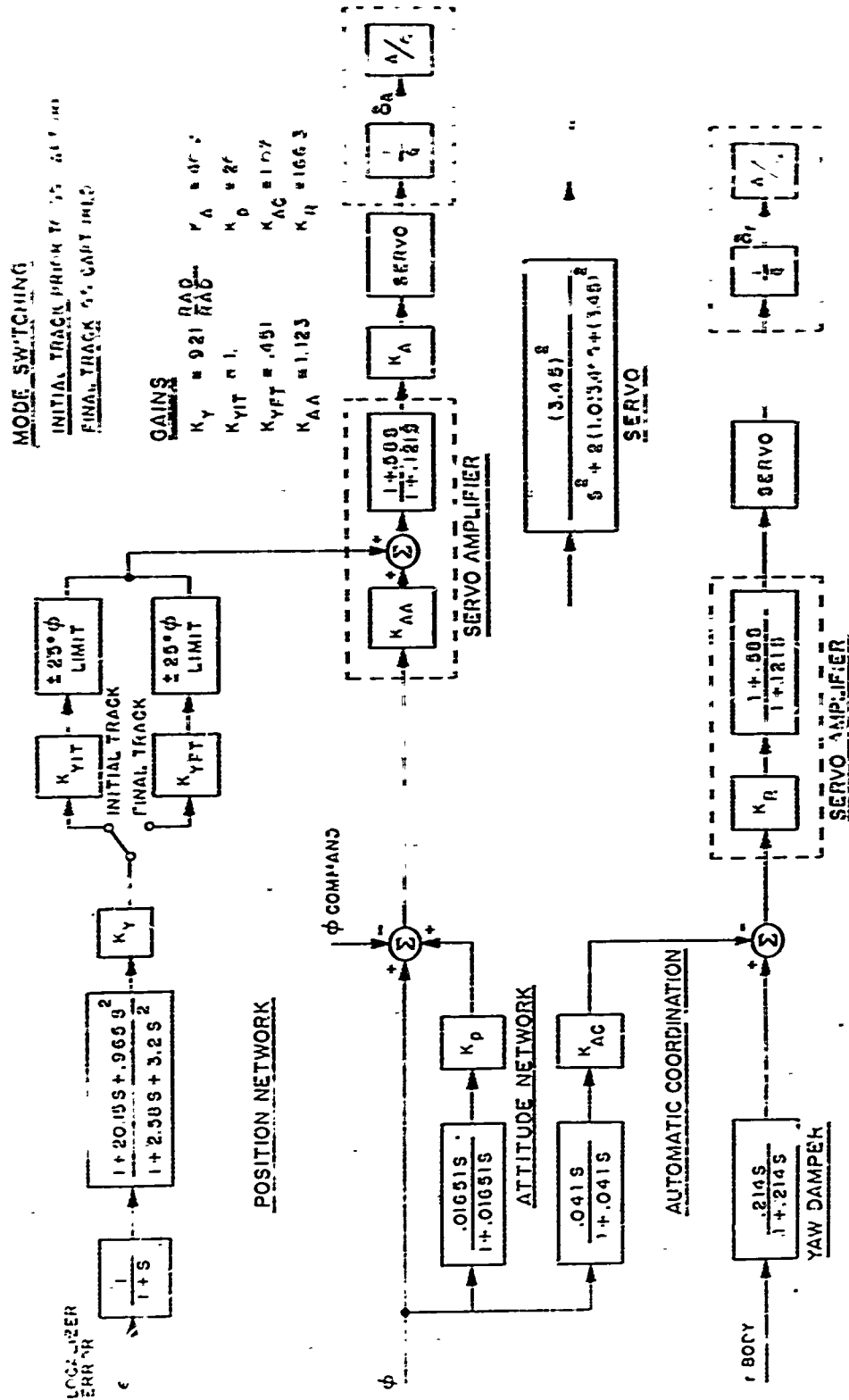
Figure 7. Lateral Control System

-16-

disengaged. To prevent a sudden pitchup at this point a 0.044 rad. nose down command is biased into the attitude circuit, to cancel the input from switch B. Thus, after engagement, the airplane will continue in level flight. As it moves closer to the glidepath, the signal at B will continue to decrease, and the bias signal will gradually pitch the nose down. The gains and logic switches are set so that the airplane gradually approaches the correct glideslope with minimal overshoot. Speed is controlled manually at all times in the representative autopilot system since auto-throttles are not typically provided. However, a preliminary auto-throttle was derived at TSC by simulation and can be used for completely automatic approach studies. The auto-throttle system is shown in Figure 8.

Figure 8. Auto-throttle

$$\tau_u = 4.\ \text{SEC}$$
$$\tau_{\theta'} = 30.\ \text{SEC}$$
$$\tau_{\theta''} = 2.\ \text{SEC}$$
$$K_{1u} = .125$$
$$K_u = 2.54$$
$$K_{\theta'} = 62.9$$

-18-
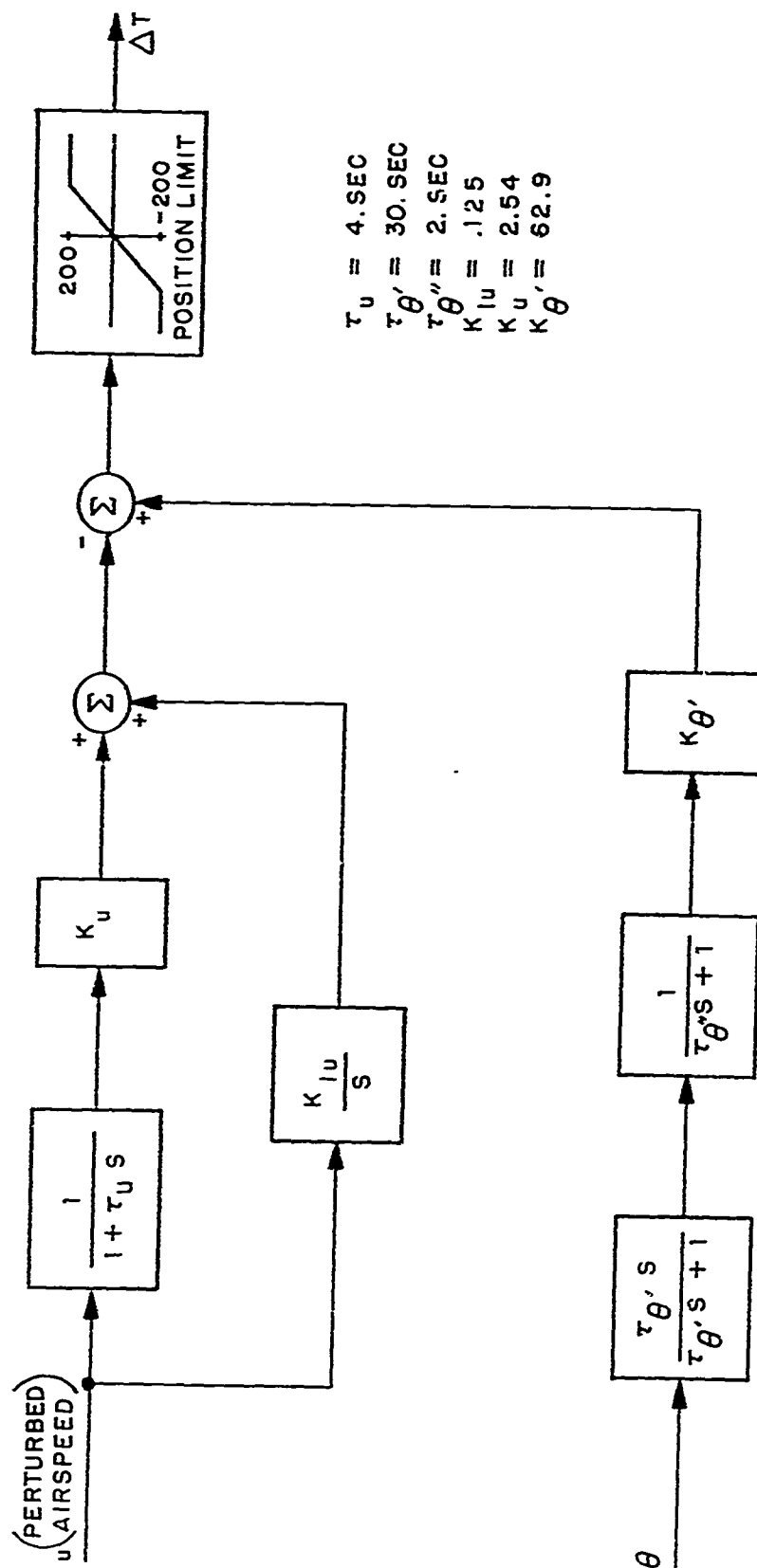
5. INSTRUMENT PANEL[5]

The instrument panel layout is shown in Figure 9. It is designed to accommodate the customary advanced flight instruments on the left side in front of the pilot and engine instruments on the right side.
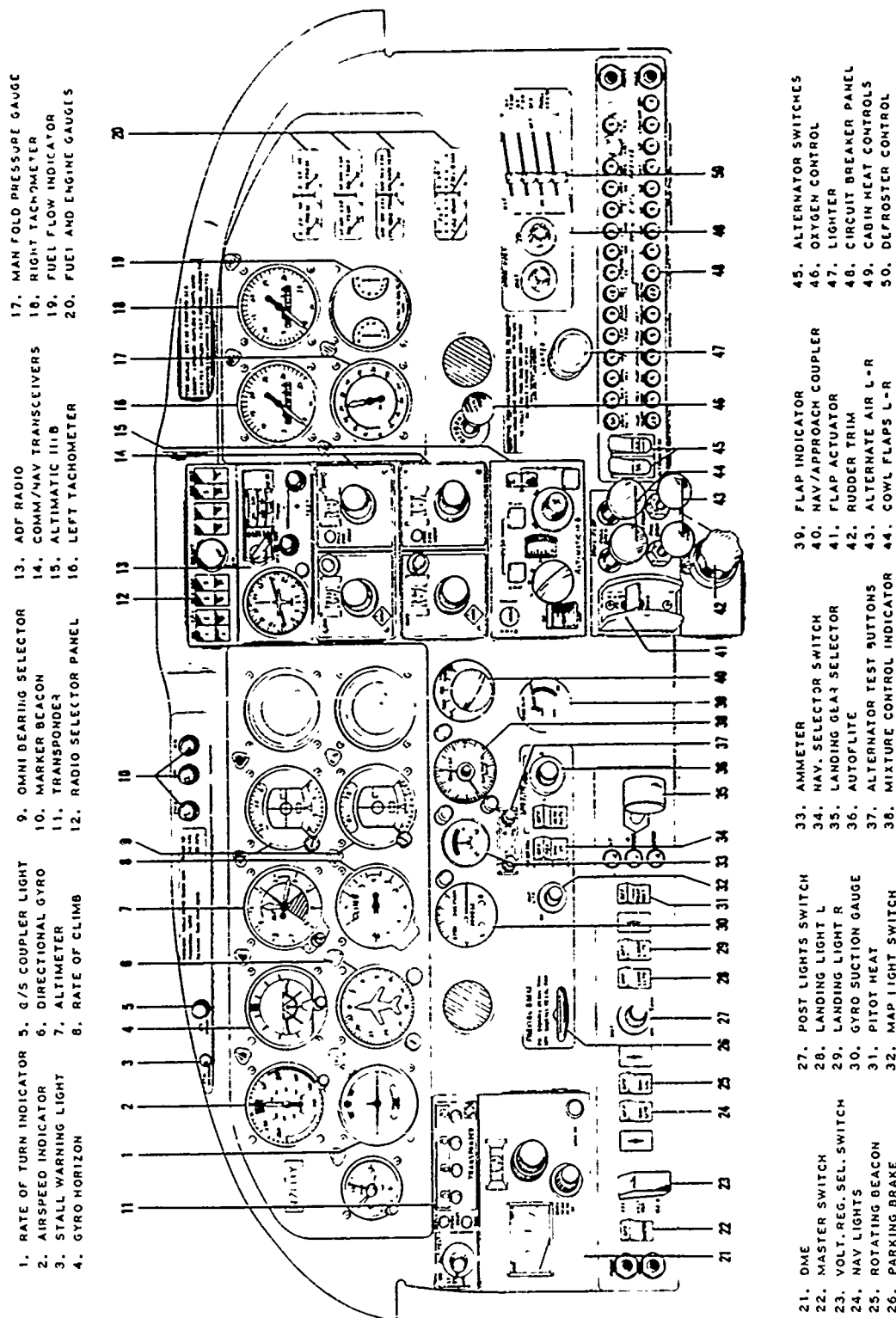
-19-

1. RATE OF TURN INDICATOR
2. AIRSPEED INDICATOR
3. STALL WARNING LIGHT
4. GYRO HORIZON

5. G/S COUPLER LIGHT
6. DIRECTIONAL GYRO
7. ALTIMETER
8. RATE OF CLIMB

9. OMNI BEARING SELECTOR
10. MARKER BEACON
11. TRANSPONDER
12. RADIO SELECTOR PANEL

13. ADF RADIO
14. COMM/NAV TRANSCEIVERS
15. ALTIMATIC IIIB
16. LEFT TACHOMETER

17. MAN FOLD PRESSURE GAUGE
18. RIGHT TACHOMETER
19. FUEL FLOW INDICATOR
20. FUEL AND ENGINE GAUGES

21. DME
22. MASTER SWITCH
23. VOLT. REG. SEL. SWITCH
24. NAV LIGHTS
25. ROTATING BEACON
26. PARKING BRAKE

27. POST LIGHTS SWITCH
28. LANDING LIGHT L
29. LANDING LIGHT R
30. GYRO SUCTION GAUGE
31. PITOT HEAT
32. MAP LIGHT SWITCH

33. AMMETER
34. NAV. SELECTOR SWITCH
35. LANDING GEAR SELECTOR
36. AUTOFLITE
37. ALTERNATOR TEST BUTTONS
38. MIXTURE CONTROL INDICATOR

39. FLAP INDICATOR
40. NAV/APPROACH COUPLER
41. FLAP ACTUATOR
42. RUDDER TRIM
43. ALTERNATE AIR L-R
44. COWL FLAPS L-R

45. ALTERNATOR SWITCHES
46. OXYGEN CONTROL
47. LIGHTER
48. CIRCUIT BREAKER PANEL
49. CABIN HEAT CONTROL
50. DEFROSTER CONTROL

Figure 9. Instrument Panel Layout

-20-

REFERENCES

1. Koziol, Joseph, <u>Manueverability of Conventional Fixed Wing Aircraft in the Landing Approach</u>, In-House Memorandum, December 15, 1970

2. Koziol, Joseph, <u>Selection of a Representative Light Maneuverable Aircraft for Instrumented Approach and Landing Studies</u>, In-House Memorandum August 13, 1970

3. Koziol, Joseph, <u>A Comparison Between the Cessna 310 and the Piper PA-30 Twin Comanche</u>, In-House Memorandum, October 6, 1970

4. Fink, P. Marvin, and Delma C. Freeman, Jr., <u>Full-Scale Wind-Tunnel Investigation of Static Longitudinal and Lateral Characteristics of a Light Twin-Engine Airplane</u>, NASA TN D-4983, January, 1969.

5. <u>Piper Twin Comanche Owner's Handbook</u>, Part No. 753 773, January, 1970

6. Kohlman, David L., <u>An Analytical Description of Typical Light Airplane Autopilot and Control Systems</u>, Prepared for TSC under Purchase Order No. TS-578, December 14, 1970.